Atmos. Chem. Phys. Discuss., 11, 1153–1188, 2011
www.atmos-chem-phys-discuss.net/11/1153/2011/
doi:10.5194/acpd-11-1153-2011

Atmospheric Chemistry and Physics Discussions

Aerosol particle number size distributions and particulate light absorption at the ZOTTO tall tower (Siberia), 2006–2009

J. Heintzenberg[1], **W. Birmili**[1], **R. Otto**[1], **M. O. Andreae**[2], **J.-C. Mayer**[2], **X. Chi**[2], **and A. Panov**[3]

[1]Leibniz-Institute for Tropospheric Research, Permoserstr. 15, 04318 Leipzig, Germany
[2]Max-Planck-Institute for Chemistry, Joh.-Joachim-Becher-Weg 27, 55128 Mainz, Germany
[3]VN Sukachev Institute of Forest, Siberian Branch/Russian Academy of Science, Akademgorodok, Postbox 26695, 660036 Krasnoyarsk, Russia

Received: 17 December 2010 – Accepted: 4 January 2011 – Published: 17 January 2011

Correspondence to: J. Heintzenberg (jost@tropos.de)

Published by Copernicus Publications on behalf of the European Geosciences Union.

Abstract

This paper covers measurements of the number-size distribution of aerosol particles, particulate absorption at 570 nm wavelength and CO as tracer gas from 2006 through 2009 at 50 and 300 m on the ZOTTO tower, Siberia at 60.8° N; 89.35° E. Average number, surface and volume concentrations are similar to results given for continental and boreal background locations. When fitted with lognormal functions, the probability distribution function of modal diameters shows three main maxima in the Aitken and accumulation size range and a possible secondary maximum in the nucleation size range below 25 nm. The seasonal distributions of the different particle parameters differ substantially. Particulate absorption has a clear single maximum in high winter and minimum values in mid-summer. The 90%-percentile, however, indicates a possible secondary maximum in July/August that may be related to forest fires. The strongly combustion derived CO shows a single winter maximum and a late summer minimum, albeit with a considerable smaller seasonal swing than the particle data due to its longer atmospheric lifetime. Total volume and even more so total number show a more complex seasonal variation with maxima in winter, spring, and summer. A cluster analysis of back trajectories complemented by local stability information yielded ten clusters with three levels of particle concentration: Low concentrations for the northernmost (Arctic) clusters mid-level concentrations for clusters reaching rapidly west between 55° and 65° latitude, and high concentrations for the cluster reaching southwest via Kazakhstan to the central Russian industrial region.

1 Introduction

Siberia is currently poorly represented in the system of global atmospheric observations. The lack of surface-based observations concerns especially the properties and potential climate effects of atmospheric aerosol particles. The paucity of observations is highly contradictory to the global relevance of the Siberian landmass as a source

ACPD
11, 1153–1188, 2011

and sink for aerosol particles, and their role in the global radiation budget. The major natural aerosol sources over Siberia include forest fires (Vivchar et al., 2011) as well as secondary aerosol formation from gaseous precursors as was observed over other boreal forests (Dal Maso et al., 2005; Kristensson et al., 2008; Pryor et al., 2008). The 300 m tall meteorological tower facility ZOTTO was erected 2006 near Zotino, Russia, in the heart of the Siberian ecosystem. At this site, anthropogenic influences are of minor importance, so that the sampled aerosol can be representative for a very large spatial area. A study of the representativeness of the ZOTTO facility and first overviews and analyses of the particle size distribution data can be found in Heintzenberg et al. (2008) and Heintzenberg and Birmili (2010). The present report covers a statistical analysis of aerosol data taken through the first four years of operation of the ZOTTO facility. Beyond the size distribution it includes measurements of particulate absorption and CO as a tracer gas. With a cluster analysis of back trajectories seasonally dependent major air mass pathways and related aerosol size distributions are determined.

2 Instrumental

2.1 The Zotino Tall Tower Facility (ZOTTO)

Since 2006, a unique research platform is available in Central Siberia as the Zotino Tall Tower Facility (ZOTTO) at 60.8° N; 89.35° E, about 20 km west of the Yenisei river. The site lies in a vast region of forests and bogs, still relatively undisturbed by anthropogenic influences and relatively inhospitable because of its continental climate. The population density is low but a moderate human impact on vegetation, e.g., by logging activities, is already visible. The climate is dominated by a large seasonal temperature cycle spanning from minima below −55 °C in winter to maxima above 30 °C in summer. The tower is 300 m high and was designed for long-term atmospheric observations in Siberia that are representative for a very large spatial area. A significant benefit of tall tower sampling is also that measurements aloft are less prone to contamination by unavoidable local sources such as the power generator of the facility.

ACPD
11, 1153–1188, 2011

The tower and the adjacent underground laboratory were constructed between 2004 and 2006 by the Max Planck Society (http://www.bgc-jena.mpg.de/bgc-systems/projects/zotto/index.shtml). The scientific leader of the ZOTTO facility is the Max Planck Institute for Biogeochemistry in Jena, Germany, and the VN Sukachev Institute of Forest, Krasnoyarsk, Russia, together with the Max Planck Institute for Chemistry, Mainz, Germany. The VN Sukachev Institute of Forest continually operates and maintains the ZOTTO facility. More details of the ZOTTO facility are given in Kozlova et al. (2008, 2009).

Trace gas measurements obtained by aircraft in summer in the Zotino area (Lloyd et al., 2002) indicated a well mixed planetary boundary layer by the depletion of carbon dioxide concentration as a result of daytime photosynthesis. This measurement shows that a 300 m sampling point on the tower should be largely representative for boundary layer air, thereby avoiding effects that are related to the shallow surface layer, indicated by an excess in biogenic oxygen isotopes. Further arguments for the suitability of ZOTTO for background measurements can be found in Winderlich et al. (2010).

2.2 The aerosol inlet at ZOTTO

Ambient aerosols at ZOTTO are collected through two inlet pipes, one reaching to the top of the tower at 300 m above ground, the other one to 50 m height. A computer-controlled valve system switches the aerosol sampling between the two levels every six minutes while maintaining the nominal 40 l min^{-1} flow in both inlets. The details of the experimental set-up including a calibration of the inlet for particle losses are described in a specialized paper (Birmili et al., 2007) and in Heintzenberg et al. (2008). Briefly, particles with diameter (D_p)>50 nm and less than 1 µm are nearly perfectly transmitted through the pipe, and 10 nm particles are still transmitted at a reproducible efficiency of 20%. The calibration and the related numerical calculations were used in this paper to correct all particle size distributions for the transmission losses occurring in the sampling pipes.

ACPD
11, 1153–1188, 2011

2.3 Size distribution measurements

Particle number size distributions in the diameter range 12–835 nm are recorded continuously at ZOTTO by a Differential Mobility Particle Sizer (DMPS). The instrument has been optimized in several ways for the special requirements of long-term operation at ZOTTO: automatic and largely unattended operation, low level of maintenance, long-term stability, avoidance of radioactive sources as a charging device.

Specifically, the DMPS uses a Hauke-type differential mobility analyzer (DMA) with a center rod length of 28 cm (Winklmayr et al., 1991). Positive voltages up to 12 500 kV are applied, thus selecting negatively charged particles in the DMA. Particles downstream of the DMA are counted with a laminar flow condensation particle counter (CPC model 3762, TSI Inc., St. Paul, USA). The sample flow through the particle counter is limited by a critical orifice to $0.8 \pm 0.1\,\mathrm{l\,min^{-1}}$. Single particles in the CPC are counted by digital data acquisition to provide an accurate concentration measure even in the case of very low particle concentrations. A sheath-airflow of $5\,\mathrm{l\,min^{-1}}$ is circulated in a closed loop, regulated by a computer-controlled air blower with adjustable rotational frequency. Any changes to the sheath-air in terms of relative humidity (RH) are damped by an adsorption dryer with silica gel as an adsorbing agent. Due to the relative dryness of ambient air sampled in Siberia, we observed no critical accumulation of moisture in the circulated sheath air – in fact, RH stayed below 30% in the sheath air circuit at all times.

Legal restrictions prevent the deployment of a radioactive source as an aerosol neutralizer; therefore, ambient aerosol particles are neutralized in a corona-discharge based aerosol neutralizer (Stommel and Riebel, 2004). This aerosol neutralizer consists of an aerosol chamber with an AC electrical discharge and was shown to perform in an equivalent fashion to the more common Kr^{85} neutralizer in ambient aerosol measurements. The time resolution of the DMPS is about 6 min. After each measurement, the instrument switches between the 300 m and 50 m height levels to provide size distributions as a function of height.

ACPD
11, 1153–1188, 2011

After the multiple charge inversion and the particle loss corrections for the 300 m and 50 m inlet pipes (Birmili et al., 2007), the resulting particle size distributions encompasses 18 logarithmically equal size bins between 15 and 835 nm. This particle size range roughly encompasses the accumulation mode (100–835 nm), representative for aged atmospheric aerosols, the Aitken mode (50–100 nm) – representative for young aerosol particles only a few days old, and the nucleation mode (<50 nm), representing the most recently formed aerosol particles.

Unfortunately, the aerosol neutralizer failed due to electrical problems during a lengthy period between February 2008 and April 2009, during which the DMPS was operated without neutralizer. Normally, the use of a charge neutralizer is mandatory in conjunction with a DMPS, since otherwise, the state of charging is poorly defined. However, it is known that aerosol particles reach the bipolar charge equilibrium after a sufficient residence time in the atmosphere. Gagné et al. (2008) examined the charging state of environmental particles over a boreal forest using a DMPS with and without a charge neutralizer. Their one-year observations suggest that deviations from the bipolar charge equilibrium play a role in the size range of the smallest particles (<10 nm) only. Apparently, nucleation mode particles readily reach the charge equilibrium after a residence time of only a few hours in an atmospheric setting comparable to ZOTTO with respect to latitude and the biogenic ecosystem.

Using our own equipment, we conducted similar DMPS experiments in urban ambient air in Leipzig (Germany). During three days we made alternative measurements with and without the use of a Kr^{85} neutralizer using a positive DMA voltage. The main result was that in their ambient state, the urban ambient particles appeared to be undercharged, with efficiencies of 79%, 90%, and 80% at the diameters 15, 80, and 800 nm, respectively, compared to the bipolar charge equilibrium. Our conclusion is that the concentration measured by the ZOTTO DMPS during the period Febuary 2008–April 2009 might be too low by 20% at most. This estimate seems to be justified by the large distance of the ZOTTO site to the emission sources of fresh anthropogenic aerosols.

ACPD
11, 1153–1188, 2011

2.4 Particulate absorption measurements

A single-wavelength Particle/Soot Absorption Photometer (PSAP, Radiance Research, Seattle, USA) was used in this study for measuring particulate light absorption. This method is based on the integrating plate technique, in which the change in optical transmission through a filter caused after particle deposition on the filter is related to the light absorption coefficient of the deposited particles.

$$\sigma_0 = \frac{A}{V} \ln\left(\frac{\mathrm{Tr}_{t-\Delta t}}{\mathrm{Tr}_t}\right)$$

where A is the area of the sample spot, V is the volume of air drawn through area A during a given time period Δt, $\mathrm{Tr}_{t-\Delta t}$ and Tr_t are the filter transmissions before and after the time period, and σ_0 is the raw or uncorrected absorption coefficient from the PSAP. However, it is known that this equation does not directly give the accurate aerosol absorption coefficient, because of the inherent errors caused by multiple scattering effects within the filter matrix and the light scattering by the collected particles (Bond et al., 1999; Virkkula et al., 2005).

Several empirical methods have been suggested and modified for correcting these artifacts (Bond et al., 1999; Weingartner et al., 2003; Virkkula et al., 2005). In this study we corrected our data for the scattering artifact as well as calibration error after Virkkula et al. (2005). The particulate absorption coefficient was calculated from

$$\sigma_{\mathrm{AP}}(\mathrm{PSAP}) = (k_0 + k_1(h_0 + h_1\omega_0)\ln(\mathrm{Tr}))\sigma_0 - s\sigma_{\mathrm{SP}}$$

where k_0, k_1, h_0, h_1, and σ are the constants listed in Table 3 of Virkkula et al. (2005) for a single-wavelength PSAP (λ=574 nm), Tr is the Transmission of the light through the filter, represents the scattering coefficients (λ=574 nm), ω is the single-scattering albedo calculated using the iterative procedure (Eqs. 7–9, and Table 3) described in Virkkula et al. (2005). It has been estimated that this type of empirical corrections limits the overall accuracy of PSAP measurements to ca. 20–30% (Bond et al., 1999).

ACPD
11, 1153–1188, 2011

Such estimates of the uncertainty in PSAP absorption are derived from laboratory measurements, typically made using non-absorbing (e.g., ammonium sulfate) or strongly absorbing (e.g., soot, nigrosin dye) particles, which are all solid when dry (Bond et al., 1999; Virkkula et al., 2005). Some later laboratory and field experiments (Cappa et al., 2008; Lack et al., 2008) suggested that the actual uncertainty in PSAP measurements in the field is likely to be significantly larger than 20–30%. The minimum detection limit (MDL) of the PSAP was estimated to be 0.025 M m^{-1} for our hourly-average data, based on two times the standard deviation of 1-min noise (with 60 s cycle time) reported in Virkkula et al. (2005) and adjusting for our longer averaging time.

At the site, the PSAP was attended regularly, and the filter was changed when the transmission had decreased to 0.7. The aerosol flow through the instrument varied slightly around a value of 0.3 l min^{-1}. The exact flow rate (average of at least three measurements) was measured every time the filter was changed, and was used for the sampling volume calculation. The measured diameter of the sampling spot on several filters was 5.2 mm, which differs from the value of 5.0 mm given in the PSAP manual. In synchrony with the valve switching between the 300 m and 50 m height levels every 6 min, the filter transmission (Tr) from PSAP is recorded in the beginning and at the end of each individual sampling period (either for 300 m or 50 m height levels).

Our initial intention was to calculate the absorption coefficient during each of these time periods using the equations mentioned above, and then to derive separate 1-h averages for the two heights. However, it was found that this approach caused unacceptable noise due to instrumental instabilities related to humidity and pressure fluctuations. To eliminate this effect, we first calculated the hourly absorption coefficient for air mixed from both sampling levels, using the transmission at the beginning and end of the hour and the total air volume that has passed the filter during this time. We then estimated the absorption values at 50 m and 300 m height levels based on the scattering coefficients for the two height levels, which were measured independently by an integrating nephelometer (assuming ω_0 for the two height levels being identical within 1 h). The particulate scattering in this study was measured using a TSI

ACPD
11, 1153–1188, 2011

three-wavelength nephelometer (Model 3653 TSI, St. Paul, MN, USA) that measures at 450 nm, 550 nm, and 700 nm. The scattering coefficients were corrected for illumination non-idealities according to Anderson and Ogren (1998) and interpolated to 574 nm using the nephelometer-derived scattering Ångström exponent (Virkkula et al., 2005).

2.5 Carbon monoxide measurements

The CO mixing ratios were measured by UV resonance fluorescence, using a Fast-CO-Monitor (Model AL 5002, Aerolaser GmbH, Germany). Prior to measurement, the air was dried using a Nafion drier. Automated periodic zero and span calibrations were made to account for instrumental drift. The instrument was calibrated using a CO standard gas purchased from Scott-Marrin Inc. (Riverside, Cal., USA). The CO mixing ratio in this cylinder was determined to be 187.4 ppt at the Max Planck Institute for Biogeochemistry (Jena, Germany) by calibration against standards from the WMO Central Calibration Laboratory (CCL; at 21 NOAA/ESRL/GMD) (Kozlova and Manning, 2009). The original CO data, measured with a frequency of 3 s, was converted to 1-h averages to minimize uncertainties inherent in the data analysis methodology. Quality control of the continuous CO data was done by a bivariate regression analysis against independently measured data from flask samples, analyzed at the Max Planck Institute for Biogeochemistry. The regression analysis revealed a very good agreement of the two independent datasets, with an intercept of 5.1±4.2 and a slope of 0.97±0.03 (±1 standard error). A negligibly small offset is therefore obtained at ambient concentrations around typically observed values of 80–200 ppb.

3 Results

3.1 Aerosol statistics

The present data set covers the time period from September 2006 to January 2010 with several interruptions due to technical reasons and logistic constraints as indicated by the time series of daily averages of all parameters in Fig. 1.

ACPD
11, 1153–1188, 2011

3.1.1 Integral parameters

Statistics of total number, surface and volume concentrations are collected in Table 1, both as annual averages and for the summer months May–August and the winter months November–February. As discussed in the first report (Heintzenberg et al., 2008), the concentration levels are similar to results given for continental and boreal background locations, and in the range of number concentrations given for nonurban Siberian positions along the Trans-Siberian Railroad by Vatiainen et al. (2007). They are higher, however, than the concentrations at truly pristine sites (Andreae, 2009), indicating a contribution from anthropogenic sources.

For all integral parameters and all seasons the concentrations are higher at 50 m than at 300 m, with their ratio being highest in number and lowest in volume concentrations. This suggests the measurement at 50 m to be influenced in a stronger fashion by particle sources. At both heights, median number and surface concentrations in summer are 10 to 20% higher in summer than in winter, whereas volume concentrations are 10% lower at 50 m in summer that in winter. At 300 m only the cleanest 25% of volume concentrations are 10% lower in summer than in winter.

The summer/winter differences in Table 1 suggest a closer look at the seasonal variation of the integral aerosol parameters, which we present for 300 m height in terms of monthly percentiles for total number and volume concentrations in Fig. 2. Particle number shows three maxima in winter, spring, and summer, whereas total volume only exhibits a double maximum in winter and summer. We hypothesize that the winter maxima are due to northern hemispheric fossil fuel combustion whereas frequent forest fires most likely cause the summer maxima over Siberia (Soja et al., 2004a,b; Achard et al., 2006; Vivchar et al., 2011). In boreal environments, new particle formation has been found to occur most frequently in spring (Kulmala et al., 2004). Thus, we speculate that the spring number maximum at ZOTTO in Fig. 1 is due to regional formation of ultrafine particles that do not add significant particulate mass that would show up strongly in the volume concentrations.

ACPD
11, 1153–1188, 2011

Particulate absorption as measured with the PSAP is an integral aerosol parameter that is strongly related to combustion sources. In Fig. 3 we present monthly percentiles of σ_{ap} for comparison with the annual course of the DMPS data. Particulate absorption shows a smooth seasonal variation with a high winter maximum and a broad summer minimum. The 10% percentile evens out in August whereas the 90% percentiles indicate the occurrence of elevated concentrations in June/July, consistent with the forest fire emissions we speculated about above. The monthly medians of particulate absorption are always lower at 300 m than at 50 m (not shown).

Kozlov et al. (2008) found that the mass fraction of black carbon in sub-micrometer aerosol can serve as an indicator of influence of smoke from remote forest fires in Siberia. Their long-term study revealed that this fraction in smoke of remote forest fires is lower than in the background aerosol, i.e. this smoke is less absorbing. We used total volume concentration V as a proxy for sub-micrometer mass concentrations and plotted the ratio σ_{ap}/V in Fig. 3. This ratio neatly follows absolute particulate absorption coefficients with a minimum during June/July when we suspected a maximum likelihood of regional forest fires.

CO measurements were only operational during three of the four years of the present report (and no CO data in any month of June). However, the CO results exhibit a smooth seasonal variation in Fig. 4 with a maximum during the late winter when total volume and σ_{ap} peaked and a broad minimum during the period spring through fall (lowest values in July). Like soot and other particulate matter, CO is a tracer for combustion processes, especially for biomass burning. However, due to its longer lifetime in the atmosphere and the presence of a substantial global background concentration, the seasonal swing of CO is substantially smaller than that of σ_{ap} leading to a clear summer maximum in the ratio CO/σ_{ap} in Fig. 4. The spring and summer peaks in number concentrations suggest substantial new particle formation.

ACPD
11, 1153–1188, 2011

3.1.2 Particle size distributions

For the statistical analysis the 18 size-channel particle size distributions were reduced to nine parameters each by fitting three lognormal functions (Heintzenberg, 1994) to any measured distribution, starting from hourly median data. The fitting algorithm programmed in FORTRAN utilized a random search of a given space of geometric standard deviations σ_g of $1.1 \leq \sigma_g \leq 2.3$ and geometric mean diameters D_g of $10 \leq D_g \leq 1000$ nm combined with a least square fit of total number concentrations N_m (m=1, 3) within each of the three modes. Within each fitting process the number of modes was minimized while maintaining the constraint of 20% relative deviation between measured and fitted data.

The probability distribution functions (pdf) of D_g at both, 50 m and 300 m, and the size distribution of median σ_g at both elevations drawn in Fig. 5 clearly show that the shape of the size distributions is quite similar at both, 50 m and 300 m. Most frequent geometric mean diameters are found (with decreasing probability) at 300 nm, 150 nm, and 40 nm. The broadest lognormal modes are found around 100 nm with geometric standard deviations σ_g decreasing towards both, smaller and larger particle sizes.

Figure 6 compares percentiles of the fitted number size distributions at 300 m height in the three summer months May through August with the winter months November through February. The median size distributions for the 5% smallest and the 5% of the largest values of the total number concentrations are given for both seasons. The respective total particle numbers in summer were 290 and 4100 cm^{-3} in summer, and 220 and 3400 cm^{-3} in winter. In summer more large-Aitken and/or small-accumulation mode particles occur, whereas in winter considerably more small-Aitken and large-accumulation mode particles are found in both extreme sub-populations. The prominent occurrence of a mode at about 100 nm in the size distribution of the largest concentration periods in summer (full red line in Fig. 6) agrees with a strong contribution from biomass burning during this season, as this is the typical modal size of relatively fresh biomass smoke (e.g., Guyon et al., 2005; Reid et al., 2005). The cleanest air

ACPD
11, 1153–1188, 2011

masses in winter carry considerable more particulate volume (particles>100 nm diameter) than the cleanest summer air.

Monthly medians of the modal concentrations N_m and the geometric mean diameters D_g shed some more light on the seasonal aerosol variations than visible from the integral parameters discussed in Sect. 3.1. In Fig. 7 first (30–40 nm) and second modes (100–130 nm) to some extent follow the annual course of the integral size distribution parameters N, S, and V as shown in Fig. 2. As expected from that figure the absolute seasonal variations of all three modes in both concentrations and size are not very large. Both, mode 2 and mode 3 have a broad minimum in late summer and fall. Mode 2 has a wide maximum connecting winter and early summer whereas mode 3 has a clear late winter maximum, typical for Arctic haze. The smallest particles, fitted by mode 1, have their smallest monthly median concentrations in the summer months June through August while their geometric mean diameters also are smallest. Because of high concentrations of ultrafine particles (<25 nm) being rather rare at ZOTTO we also display monthly 90% percentiles of N_1 in Fig. 7, showing highest values around 1000 cm^{-3} for the months February through June.

3.2 Back trajectory cluster analysis

Back trajectory analysis has been shown to be a powerful tool to analyse atmospheric observations at a receptor point with respect to synoptic-scale transport processes. Since the late 1980s back trajectory cluster analysis has been applied to statistically analyse atmospheric flow patterns in primarily oceanic (Harris and Kahl, 1990; Dorling and Davies, 1995), polar regions (Harris, 1992; Harris and Kahl, 1994), and continental (Owega et al., 2006) environments. The method has also proved successful in explaining trace gas observations (Cape et al., 2000) as well as near-surface aerosol concentrations (Oriol et al., 2004; Abdalmogith and Harrison, 2005; Borge et al., 2007) including new particle formation (Charron et al., 2007; Dal Maso et al., 2007). A key advantage of trajectory analysis over a manual synoptic analysis is the automated data treatment.

ACPD
11, 1153–1188, 2011

Previous work confirmed that the mixed layer height is instrumental in explaining near-surface aerosol concentrations in continental regions (Schäfer et al., 2006; Engler et al., 2007; Birmili et al., 2010). In summer, there is a significant diurnal cycle in surface temperature over the large landmass of Siberia, which leads to convection and a well-mixed planetary boundary layer with heights up to 2 km (Koutsenogii, 1997; Paris et al., 2009). In the absence of remote-transported aerosol layers, the concentrations of particles and trace gases will consequently be lower in the afternoon because the mixing volume increases. The presence of an inversion, aerosols emitted from near the surface can be trapped in a rather small volume. In practice, the vertical gradient of the pseudo-potential temperature θ_v can be used to decide whether an air parcel has the ability to move and disperse vertically. In a cluster analysis, information on vertical stability can be incorporated in the shape of profiles of θ_v (Engler et al., 2007; Birmili et al., 2010). Besides back trajectories, however, information from radio soundings was incorporated in our analysis because of the crucial role of the vertical atmospheric stratification in near-surface atmospheric measurements. Trajectory simulations on a coarse global grid cannot capture this local effect.

3-D-backward trajectories were calculated for the years 2006–2009 using a PC-version of HYSPLIT, a trajectory model provided by the Air Resources Laboratory (ARL) of NOAA (Draxler and Rolph, 2003). Back trajectories were calculated from the GDAS analysis set, which has meteorological fields every 3 h, a spatial horizontal resolution of 1°, and a vertical resolution corresponding to the standard pressure levels (1000, 925, 850 hPa, etc.). Backward trajectories reaching 144 h back in time were computed for ZOTTO at the starting levels of 300, 1000 and 2000 m above the ground. Although the trajectories were computed for four times a day, only the 19:00 LT trajectory was analysed further for consistency with the radio sounding analyses as outlined below. Due to computational problems at the 300 m trajectory level (trajectories hitting the ground), we used back trajectories starting at the 1000 m level only.

For our present study, we also employed radio soundings from the station Bor (61.6° N, 90.01° E, 58 m a.s.l.), about 100 km north of ZOTTO, which we assume to

ACPD
11, 1153–1188, 2011

be representative for ZOTTO as well. Radio soundings at Bor are available daily at 07:00 and 19:00 LT. Due to the gradual development of vertical mixing through the day, measurements in the afternoon will be more representative for the entire boundary layer, and also for a wider horizontal area. For this reason, our trajectory cluster analysis focuses on aerosol measurements recorded in the afternoon, using solely the 19:00 LT radio sounding for the cluster analysis. To provide DMPS data corresponding to the 19:00 LT radio sounding and back trajectory, particle number size distributions were averaged for the period between 14:00–20:00 LT.

For vertical air exchange, not the absolute values of θ_v are important but its vertical gradient. To make the vertical profiles comparable throughout all seasons, all profiles were normalised to 0 °C at a fixed height above ground. To avoid interference with very surface-related phenomena (such as local overheating), this critical height was set to 300 m a.g.l.

The trajectory-clustering algorithm was a modification of the algorithm version used before for particle size distribution analysis (Engler et al., 2007; Birmili et al., 2010). It is principally based on the approach of Dorling et al. (1992). The algorithm uses the *k*-means method, i.e. a fixed number of *k* trajectory clusters is defined prior to analysis. The algorithm aims at minimizing the distances between each object (3-D-trajectory plus θ_v profile) to its cluster mean while maximizing the distances between all cluster means. In other words, trajectories are to be clustered in bundles as narrow as possible, with the mean trajectories in all bundles being as different as possible. As a measure for the distance *D* between two objects, the following expression was used:

$$D = \Sigma_i [k_i * ((w_\beta * \Delta\beta_i)^2 + (w_z * \Delta z_i)^2 + (w_\theta * \Delta\theta_i)^2)].$$

Here, $\Delta\beta$ is the distance between two trajectory points in degrees in spherical coordinates, Δz the distance between trajectories in the vertical dimension (height z), and $\Delta\theta$ the difference between two corresponding points in the vertical profiles of θ_v. All squared distances are summarised over the entire length of the trajectory (index i), weighted with a distance factor k_i. (In analogy for the θ_v profiles, all i values corresponding to levels between 300 m to 3300 m above the surface were summarized.)

ACPD
11, 1153–1188, 2011

The distance factor k_i was set to 1 at the start of the trajectory, and 0 at the end of each trajectory, linearly interpolating in between. (In analogy for the θ_v profiles, the factor was one near the surface, and zero far aloft.) The distance factor ensures that distances between trajectories far from the ZOTTO site are not overemphasized. To make horizontal and vertical trajectory distances as well as distances in θ_v comparable both in magnitude and units, these were multiplied by the appropriate weights w_β (in $1/^\circ$), w_z (in $1/\mathrm{m}$), and w_θ (in $1/\mathrm{K}$).

In a first step, the cluster algorithm assigns all trajectories to one of the k pre-defined clusters based on the minimum distance D between the trajectories (and also radio sounding data). Specifically, the pre-defined clusters involved straight trajectories radiating from the ZOTTO site in different directions, thereby sharing equal segments of the 360° horizon. When all data points were allocated to their appropriate seed trajectory by the principle of the minimum distance D, new cluster mean values were calculated from all data points (trajectory points, θ_v profiles) within each cluster. Then, a new iteration was started, re-allocating all data points to the new cluster means using again minimizing D. This procedure was repeated until the allocation of data points to the k clusters converged and no more re-allocation occurred.

It is an intrinsic property of the k-means clustering method that different initialisations of the k seed trajectories, such as involving slightly different wind directions, usually yield different clustering results, i.e. allocations of trajectories. It was also expected that the use of different weighing factors w_β, w_z and w_θ would yield different clustering results. Therefore the cluster algorithm was run many times, using a span of cluster number k and different angles of the k seed trajectories. Also, a range of weights w_β, w_z and w_θ was used to check the sensitivity of the clustering results with respect to variations in these weights. In total, 3000 cluster analyses were performed, most of which yielded different trajectory cluster compositions.

With respect to the weights w_β, w_z and w_θ, we checked how efficiently the particle size distributions were separated by each cluster analysis run. We computed a spread parameter representing the standard deviation within the set of mean particle

ACPD
11, 1153–1188, 2011

size distributions resulting from each analysis, and weighted according to the number of trajectories in each cluster. If this spread parameter was high, a particular run is apparently well able to explain the particle size distributions as a function of the meteorological situation. It the spread parameter was low, the particular run was rather inefficient in splitting up the entire set of particle number size distributions. The analysis of the spread parameter yielded w_β=1, w_z=10^{-9}, and w_θ=2.2 as the optimum values to efficiently explain the variability in observed particle number size distributions. It became evident that the geographical origin of trajectories (β) and the vertical θ_v profile mattered most, whereas effects in the computed vertical trajectory motion (z) remained largely irrelevant for the explanations of the surface-based aerosol measurements.

With respect to the cluster number k, we finally made a compromise between fine resolution of spatial trajectory coverage (high k), and easily understandable display (low k). Each cluster should be understandable in terms of a synoptic situation and, preferably, also represent observations during a particular season. This yielded the number k=10, which is presented in the following.

The mean trajectories of the ten clusters obtained are displayed on a map with equidistant projection in Fig. 8. One can see that the ten mean trajectories divide the overall data set successfully according to different source regions and air mass speed. Trajectories tend to arrive at ZOTTO mainly from westerly and northerly directions as a result of the general west wind drift in mid-latitudes. One mean trajectory (cluster 2) travels the way from the Atlantic to ZOTTO during 144 h, whereas others originate from Central Asia (5, 6) and others from significantly higher latitudes (1, 8–10). Table 2 provides a comprehensive description of the ten clusters in terms of observed particle and meteorological parameters. The highest frequency, by far, was attributed to cluster 8 with 20% (cf. Table 2). The clusters 1, 3 and 7 account for more than 40% of all days included. Cluster 4 and 9 occur more rarely, each contributing no more than 5% to the entire data set.

Besides dividing the data into trajectories of different origin, the clustering algorithm also produced rather distinct mean profiles of the pseudo potential temperature θ_v (cf.

ACPD
11, 1153–1188, 2011

Fig. 9). The profiles for the clusters 1, 3, 7 and 8 indicate a neutrally stable atmosphere. A significant inversion, however, could be identified for the clusters 4, 10, 6 and 9 (in order of relevance). For each cluster, a season index was calculated, scoring days in mid-winter (15 January) as +1, and days in mid-summer (15 July) as −1, with sinusoidal interpolation in between. According to the season index, clusters 1, 3, 7, and 8 correspond mainly to summer periods, the others overwhelmingly to winter periods (see Table 2). Winter conditions prevailed especially in cluster 9, with an average temperature −31 °C and an air pressure 1034 hPa, indicating the wintry Siberian high-pressure area. It is evident that the clustering algorithm produced clusters that represent air masses advected from different directions at different speeds, and during different seasons.

Figure 9 shows the average size distribution of each of the ten clusters. In both graphs, three levels of particle concentration can be seen: Low concentrations (ca. 400 cm^{-3} in $dN/d\log D_p$) for clusters 1, 9, and 10, mid-level concentrations (ca. 800–1000 cm^{-3} in $dN/d\log D_p$) for clusters 2, 3, 4, 6, 7, and 8, and high concentrations (up to 1500 cm^{-3} in $dN/d\log D_p$) for cluster 5. Most number size distributions have a unimodal shape with a concentration maximum around 100 nm. For the lower concentration clusters, a bimodal shape tends to emerge, i.e. a shape with a more visible Hoppel minimum between the Aitken and accumulation modes.

The results for calculated total particle mass show a similar grouping: Cluster 5 shows the highest average particle mass concentration (6.6 $\mu g\,m^{-3}$), closely followed by cluster 6 (6.6 $\mu g\,m^{-3}$). It is worth mentioning that cluster 5 also shows the highest CO mixing ratio (189 ppm), and the highest aerosol absorption coefficient (1.6 $M\,m^{-1}$). The other clusters subsequently follow the order down to cluster 1, which shows the lowest particle mass concentration (1.9 $\mu g\,m^{-3}$).

A general observation is that the differences of the clusters in particle number and mass concentrations are rather modest. The total number concentration diverges by a factor of 2.8 at maximum between the clusters, the particle mass concentration by a factor of 3.4 at maximum. The slower an air mass, and the more it originates at

ACPD
11, 1153–1188, 2011

southerly latitudes, the higher the particle mass and number concentration as well as the CO mixing ratio. Anthropogenic emissions from industrial centres are suspected to contribute to the elevated concentration values particularly of the clusters 5 and 6. It is also interesting to note that biomass burning events did apparently influence the ZOTTO site during 2006–2009 so rarely that they did not greatly influence the mean particle concentrations. Also, the effects of new particle formation (at diameters <30 nm) occurred so rarely that it did not affect the observed mean concentration values (cf. Table 2). The results underline the location of ZOTTO being representative for a large spatial area and ecosystem, which is sometimes influenced by remote aerosol transport, but which apparently exhibits only a limited intensity of aerosol sources on its own.

4 Conclusions

This paper covers measurements of the number-size distribution of aerosol particles taken from September 2006 through 2009 at 50 and 300 m on the ZOTTO tower, Siberia at 60.8° N; 89.35° E. Additionally, particulate absorption at 570 nm wavelength and CO as tracer gas were measured during much of the total time period. A statistical evaluation of the combined aerosol data set allowed drawing conclusions on three issues concerning the aerosol over the large Siberian forest area: Representative integral particle properties and size distributions, the seasonal variation of the aerosol, and its possible sources.

Average number, surface and volume concentrations (and estimated mass concentrations) are similar to results given for continental and boreal background locations. They are higher, however, than the concentrations at truly pristine sites (Andreae, 2009), indicating a contribution from anthropogenic sources.

For all integral parameters and all seasons the concentrations are higher at 50 m than at 300 m, with their ratio being highest in number and lowest in volume concentrations, suggesting the measurement at 50 m to be influenced more strongly by near-surface

ACPD
11, 1153–1188, 2011

particle sources. When fitted with lognormal functions, the probability distribution function of modal diameters shows three main maxima in the Aitken and accumulation size range and a possible secondary maximum in the nucleation size range below 25 nm.

The seasonal distributions of the different particle parameters differ substantially. Median soot-related particulate absorption has a clear single maximum in high winter (February) and minimum values in mid-summer. This distribution is typical for northern hemispheric combustion related aerosol parameters as seen in the Arctic haze (Heintzenberg, 1989). The 90%-percentile, however, indicates a possible secondary maximum in July/August. The strongly combustion derived CO shows a single winter maximum and a late summer minimum, albeit with a considerable smaller seasonal swing than the particle data due to its longer atmospheric lifetime. Total volume and even more so total number show a more complex seasonal variation with maxima in winter, spring, and summer. Interestingly, the ratio particulate absorption to volume has a more clearly expressed July minimum than absorption itself, indicating the possibility of non-combustion related particle sources over the Siberian summer forest, which will be analyzed further in a follow-up paper.

Three-year statistics of back trajectories had shown that the aerosol sampled at ZOTTO is representative of about half the Russian Federation and most of the Kazakhstan Republic (Heintzenberg et al., 2008). With a cluster analysis of back trajectories complemented by local stability information, the air mass origin of the aerosol at ZOTTO was investigated further yielding ten clusters with three levels of particle concentration: Low concentrations for the northernmost (Arctic) clusters 1, 9, and 10, mid-level concentrations for clusters 2, 3, 4, 6, 7, and 8, reaching rapidly west between 55° and 65° latitude, and high concentrations for cluster 5 reaching southwest via Kazakhstan to the Central Russian industrial region. Most number size distributions have a concentration maximum around 100 nm. For the lower concentration clusters, a bimodal shape tends to emerge, i.e. with more evident Aitken and accumulation modes.

ACPD
11, 1153–1188, 2011

Acknowledgement. The Max Planck Institute established the ZOTTO facility after many years of preparatory fieldwork, planning and massive investments by the Max Planck Society in particular for Biogeochemistry in Jena. We thank E.-D. Schulze and M. Heimann (MPI Biogeochemistry), A. A. Onuchin, and S. Verchovetz, (V. N. Sukachev Institute of Forest) for their contributions to the establishment and management of ZOTTO, and Y. Kisilyakhov, A. Tsukanov (V. N. Sukachev Institute of Forest), and N. Jürgens (MPI Chemistry) for technical support. The ZOTTO project is funded by the Max Plank Society through the International Science and Technology Center (ISTC) partner project #2757p within the framework of the proposal "Observing and Understanding Biogeochemical Responses to Rapid Climate Changes in Eurasia", and by the German Research Council (DFG). We thank Steffen Schmidt and Karl Kübler (MPI Jena) for their continuous logistic assistance during the experiment. We acknowledge Ulrich Riebel (Technical University of Cottbus, Chair for Particle Technology) for generously sharing his technology of the corona discharge based aerosol neutralizer. We thank Alfred Wiedensohler (IfT Leipzig) for the fruitful discussions about environmental aerosol charging.

References

Abdalmogith, S. S. and Harrison, R. M.: The use of trajectory cluster analysis to examine the long-range transport of secondary inorganic aerosol in the UK, Atmos. Environ., 39, 6686–6695, 2005.

Achard, F., Mollicone, D., Stibig, H. J., Aksenov, D., Laestadius, L., Li, Z. Y., Popatov, P. and Yaroshenko, A.: Areas of rapid forest-cover change in boreal Eurasia, Forest Ecol. Manage., 237, 322–334, 2006.

Anderson, T. L. and Ogren, J. A.: Determining aerosol radiative properties using the TSI 3563 integrating nephelometer, Aerosol Sci. Tech., 29, 57–69, 1998.

Andreae, M. O.: Correlation between cloud condensation nuclei concentration and aerosol optical thickness in remote and polluted regions, Atmos. Chem. Phys., 9, 543–556, doi:10.5194/acp-9-543-2009, 2009.

Birmili, W., Stopfkuchen, K., Hermann, M., Wiedensohler, A., and Heintzenberg, J.: Particle penetration through a 300 m inlet pipe for sampling atmospheric aerosols from a tall meteorological tower, Aerosol Sci. Technol., 41, 811–817, 2007.

Birmili, W., Heinke, K., Pitz, M., Matschullat, J., Wiedensohler, A., Cyrys, J., Wichmann, H.-E.,

ACPD

11, 1153–1188, 2011

and Peters, A.: Particle number size distributions in urban air before and after volatilisation, Atmos. Chem. Phys., 10, 4643–4660, doi:10.5194/acp-10-4643-2010, 2010.
Bond, T. C., Anderson, T. L., and Campbell, D.: Calibration and intercomparison of filter-based measurements of visible light absorption by aerosols, Aerosol Sci. Tech., 30, 582–600, 1999.
Borge, R., Lumbreras, J., Vardoulakis, S., Kassomenos, P., and Rodríguez, E.: Analysis of long-range transport influences on urban PM_{10} using two-stage atmospheric trajectory clusters, Atmos. Environ., 41, 4434–4450, 2007.
Cape, J. N., Methven, J. and Hudson, L. E.: The use of trajectory cluster analysis to interpret trace gas measurements at Mace Head, Ireland, Atmos. Environ., 34, 3651–3663, 2000.
Cappa, C. D., Lack, D. A., Burkholder, J. B., and Ravishankara, A. R.: Bias in filter-based aerosol light absorption measurements due to organic aerosol loading: Evidence from laboratory measurements, Aerosol Sci. Tech., 42, 1022–1032, 2008.
Charron, A., Birmili, W., and Harrison, R. M.: Factors influencing new particle formation at the rural site, Harwell, UK, J. Geophys. Res., 112, D14210, doi:14210.11029/12007JD008425, 2007.
Dal Maso, M., Kulmala, M., Riipinen, I., Wagner, R., Hussein, T., Aalto, P. P., and Lehtinen, K. E. J.: Formation and growth of fresh atmospheric aerosols: eight years of aerosol size distribution data from SMEAR II, Hyytiälä, Finland, Bor. Env. Res., 10, 323–336, 2005.
Dal Maso, M., Sogacheva, L., Aalto, P. P., Riipinen, I., Komppula, M., Tunved, P., Korhonen, L., Suur-Uski, V., Hirsikko, A., Kurtén, T., Kerminen, V.-M., Lihavainen, H., Viisanen, Y., Hansson, H.-C., and Kulmala, M.: Aerosol size distribution measurements at four Nordic field stations: identification, analysis and trajectory analysis of new particle formation bursts, Tellus, 59B, 350–361, 2007.
Dorling, S. R. and Davies, T. D.: Extending cluster analysis – synoptic meteorology links to characterise chemical climates at six northwest European monitoring stations, Atmos. Environ., 29, 145–167, 1995.
Dorling, S. R., Davies, T. D., and Pierce, C. E.: Cluster analysis: a technique for estimating the synoptic meteorological controls on air and precipitation chemistry – method and applications, Atmos. Environ., 26A, 2575–2581, 1992.
Draxler, R. and Rolph, G.: HYSPLIT (HYbrid Single-Particle Lagrangian Integrated Trajectory) Model access via NOAA ARL READY. NOAA Air Resources Laboratory, Silver Spring, MD, 2003.
Engler, C., Rose, D., Wehner, B., Wiedensohler, A., Brüggemann, E., Gnauk, T., Spindler, G.,

ACPD
11, 1153–1188, 2011

Tuch, T., and Birmili, W.: Size distributions of non-volatile particle residuals (D_p<800 nm) at a rural site in Germany and relation to air mass origin, Atmos. Chem. Phys., 7, 5785–5802, doi:10.5194/acp-7-5785-2007, 2007.
Gagné, S., Laakso, L., Petäjä, T., Kerminen, V.-M. and Kulmala, M.: Analysis of one year of Ion-DMPS data from the SMEAR II station, Finland, Tellus B, 60, 318–329, 2008.
Guyon, P., Frank, G. P., Welling, M., Chand, D., Artaxo, P., Rizzo, L., Nishioka, G., Kolle, O., Fritsch, H., Silva Dias, M. A. F, Gatti, L. V., Cordova, A. M., and Andreae, M. O.: Airborne measurements of trace gas and aerosol particle emissions from biomass burning in Amazonia, Atmos. Chem. Phys., 5, 2989–3002, doi:10.5194/acp-5-2989-2005, 2005.
Harris, J. M.: An analysis of 5-day midtropospheric flow patterns for the South Pole: 1985–1989, Tellus B, 44, 409–421, 1992.
Harris, J. M. and Kahl, J. D.: A descriptive atmospheric transport climatology for the Mauna Loa Observatory, using clustered trajectories, J. Geophys. Res., 95D, 13651–13667, 1990.
Harris, J. M. and Kahl, J. D. W.: Analysis of 10-day isentropic flow patterns for Barrow, Alaska: 1985–1992, J. Geophys. Res., 99D, 25845–25855, 1994.
Heintzenberg, J.: Arctic haze: air pollution in polar regions, AMBIO, 18, 50–55, 1989.
Heintzenberg, J.: Properties of the log-normal particle size distribution, Aerosol Sci. Technol., 21, 46–48, 1994.
Heintzenberg, J. and Birmili, W.: Aerosols over the Siberian forest: the ZOTTO project, J. Cryogen. Soc. Japan, 68, 5–8, 2010.
Heintzenberg, J., Birmili, W., Theiss, D., and Kisilyakhov, Y.: The atmospheric aerosol over Siberia, as seen from the 300 meter ZOTTO tower, Tellus, 60B, 276–285, 2008.
Koutsenogii, P.: Aerosol measurements in Siberia, Atmos. Res., 44, 167–173, 1997.
Kozlov, V. S., Panchenko, M. V., and Yausheva, E. P.: Mass fraction of black carbon in submicron aerosol as an indicator of influence of smoke from remote forest fires in Siberia, Atmos. Environ., 42, 2611–2620, 2008.
Kozlova, E. A. and Manning, A. C.: Methodology and calibration for continuous measurements of biogeochemical trace gas and O_2 concentrations from a 300-m tall tower in central Siberia, Atmos. Meas. Tech., 2, 205–220, doi:10.5194/amt-2-205-2009, 2009.
Kozlova, E. A., Manning, A. C., Kisilyakhov, Y., Seifert, T. and Heimann, M.: Seasonal, synoptic, and diurnal-scale variability of biogeochemical trace gases and O_2 from a 300-m tall tower in central Siberia, Global Biochem. Cy., 22, GB4020, doi:4010.1029/2008GB003209, 2008.
Kristensson, A., Dal Maso, M., Swietlicki, E., Hussein, T., Zhou, J., Kerminen, V.-M., and Kul-

ACPD
11, 1153–1188, 2011

mala, M.: Characterization of new particle formation events at a background site in Southern Sweden: relation to air mass history, Tellus B, 60, 330–344, 2008.
Kulmala, M., Vehkamäkia, H., Petäjä, T., Dal Maso, M., Lauri, A., Kerminen, V.-M., Birmili, W., and McMurry, P. H.: Formation and growth rates of ultrafine atmospheric particles: a review of observations, J. Aerosol Sci., 35, 143–176, 2004.
Lack, D. A., Cappa, C. D., Covert, D. S., Baynard, T., Massoli, P., Sierau, B., Bates, T. S., Quinn, P. K., Lovejoy, E. R., and Ravishankara, A. R.: Bias in filter-based aerosol light absorption measurements due to organic aerosol loading: Evidence from ambient measurements, Aerosol Sci. Tech., 42, 1033–1041, 2008.
Lloyd, J., Langenfelds, R. L., Francey, R. J., Gloor, M., Tchebakova, N. M., Zolotoukhine, D., Brand, W. A., Werner, R. A., Jordan, A., Allison, C. A., Zrazhewske, V., Shibistova, O., and Schulze, E.-D.: A trace-gas climatology above Zotino, Central Siberia, Tellus, 54B, 749–767, 2002.
Oriol, J., Pérez, C., Rocadenbosch, F., and Baldasano, J. M.: Cluster analysis of 4-day back trajectories arriving in the Barcelona area, Spain, from 1997 to 2002, J. Appl. Meteor., 43, 887–901, 2004.
Owega, S., Khan, B.-U.-Z., Evans, G. J., Jervis, R. E., and Fila, M.: Identification of long-range aerosol transport patterns to Toronto via classification of back trajectories by cluster analysis and neural network techniques, Chemometr. Intell. Lab. Syst., 83, 26–33, 2006.
Paris, J.-D., Arshinov, M. Y., Ciais, P., Belan, B. D., and Nédélec, P.: Large-scale aircraft observations of ultra-fine and fine particle concentrations in the remote Siberian troposphere: New particle formation studies, Atmos. Environ., 43, 1302–1309, 2009.
Pryor, S. C., Barthelmie, R. J., Sørensen, L. L., Larsen, S. E., Sempreviva, A. M., Grönholm, T., Rannik, Ü., Kulmala, M., and Vesala, T.: Upward fluxes or particles over forests: when, where, why?, Tellus B, 60, 372–380, 2008.
Reid, J. S., Koppmann, R., Eck, T. F., and Eleuterio, D. P.: A review of biomass burning emissions part II: intensive physical properties of biomass burning particles, Atmos. Chem. Phys., 5, 799–825, doi:10.5194/acp-5-799-2005, 2005.
Schäfer, K., Emeis, S., Hoffmann, H., and Jahn, C.: Influence of mixing layer height upon air pollution in urban and sub-urban areas, Meteor. Z., 15, 647–658, 2006.
Soja, A. J., Cofer, W. R., Shugart, H. H., Sukhinin, A. I., Stackhouse, P. W., McRae, D. J., and Conard, S. G.: Estimating fire emissions and disparities in boreal Siberia (1998–2002), J. Geophys. Res.-Atmos., 109, D14S06, doi:10.1029/2004JD004570, 2004a.

ACPD
11, 1153–1188, 2011

Soja, A. J., Sukhinin, A. I., Cahoon, D. R., Shugart, H. H., and Stackhouse, P. W.: AVHRR-derived fire frequency, distribution and area burned in Siberia, Int. J. Remote Sens., 25, 1939–1960, 2004b.

Stommel, Y. G. and Riebel, U.: A new corona discharge-based aerosol charger for submicron particles with low initial charge, J. Aerosol Sci., 35, 1051–1069, 2004.

Vartiainen, E., Kulmala, M., Ehn, M., Hirsikko, A., Junninen, H., Petäjä, T., Sogacheva, L., Kuokka, S., Hillamo, R., Skorokhod, A., Belikov, I., Elansky, N. and Kerminen, V.-M.: Ion and particle number concentrations and size distributions along the Trans-Siberian railroad, Bor. Env. Res., 12, 375–396, 2007.

Virkkula, A., Ahlquist, N. C., Covert, D. S., Arnott, W. P., Sheridan, P. J., Quinn, P. K., and Coffman, D. J.: Modification, calibration and a field test of an instrument for measuring light absorption by particles, Aerosol Sci. Tech., 39, 68–83, 2005.

Vivchar, A. V., Moiseenko, K. B., Mayer, J.-C., Jürgens, N., Panov, A., Heimann, M., and Andreae, M. O.: Assessment of the regional atmospheric impact of wildfire emissions based on CO observations at the ZOTTO tall tower station in Central Siberia, J. Geophys. Res.-Atmos., submitted, 2011.

Weingartner, E., Saathoff, H., Schnaiter, M., Streit, N., Bitnar, B., and Baltensperger, U.: Absorption of light by soot particles: determination of the absorption coefficient by means of aethalometers, J. Aerosol Sci., 34, 1445–1463, 2003.

Winderlich, J., Chen, H., Gerbig, C., Seifert, T., Kolle, O., Lavrič, J. V., Kaiser, C., Höfer, A., and Heimann, M.: Continuous low-maintenance CO_2/CH_4/H_2O measurements at the Zotino Tall Tower Observatory (ZOTTO) in Central Siberia, Atmos. Meas. Tech., 3, 1113–1128, doi:10.5194/amt-3-1113-2010, 2010.

Winklmayr, W., Reischl, G. P., Lindner, A. O., and Berner, A.: A new electromobility spectrometer for the measurement of aerosol size distributions in the size range from 1 to 1000 nm, J. Aerosol Sci., 22, 289–296, 1991.

ACPD
11, 1153–1188, 2011

Table 1. 25%, 50%, and 75% percentiles of number (N), surface (S), and volume (V) concentrations at 50 and 300 m height over ZOTTO, Siberia. The statistics are given as total, for the summer months May–August, and for the winter months November–February. Ratios 50 m/300 m and summer/winter are added.

		Total			May–August			November–February			50 m	300 m
Parameter	%	50 m	300 m	50 m/ 300 m	50 m	300 m	50 m/ 300 m	50 m	300 m	50 m/ 300 m	Summer/ winter	Summer/ winter
N	25	970	750	1.3	1040	890	1.2	860	630	1.4	1.2	1.4
cm^{-3}	50	1650	1290	1.3	1630	1390	1.2	1490	1190	1.3	1.1	1.2
	75	2650	2140	1.2	2390	2110	1.1	2600	2070	1.3	0.9	1.0
S	25	66	56	1.2	79	67	1.2	67	59	1.1	1.2	1.1
$\mu m^2\,cm^{-3}$	50	120	102	1.2	128	116	1.1	113	98	1.2	1.1	1.2
	75	193	168	1.1	198	178	1.1	200	169	1.2	1.0	1.1
V	25	2.8	2.3	1.2	3.0	2.5	1.2	3.4	2.8	1.2	0.9	0.9
$\mu m^3\,cm^{-3}$	50	5.0	4.3	1.2	5.1	4.7	1.1	5.4	4.8	1.1	0.9	1.0
	75	8.7	7.6	1.1	8.9	7.9	1.1	9.8	8.3	1.2	0.9	1.0

ACPD
11, 1153–1188, 2011

Table 2. Summary of the ten trajectory clusters given as the climatological frequency (%), mean aerosol and gas concentrations, meteorological surface parameters, and the summer/winter index. The meteorological parameters were taken at the Russian meteorological service station at Vorogovo (30 km distant to ZOTTO) at 19:00 LT.

No.	Description	Freq.	N_1[1]	N_2[2]	N_3[3]	N_4[4]	N_{tot} (cm^{-3})	M[5]	CO[6]	p (hPa)	rH (%)	T (°C)	S/W[7] index
1	Arctic, summer	15%	22	100	230	80	440	1.9	139	1013	65	4	−0.3
2	Northern Europe	7%	13	150	430	140	730	3.4	152	1016	75	4	0.1
3	Northern Russia	12%	16	110	420	160	710	3.8	147	1011	68	9	−0.3
4	Central Europe, summer	4%	12	140	470	140	770	4.0	176	1022	84	−7	0.5
5	Southern latitudes	9%	25	210	720	260	1220	6.6	189	1013	82	−1	0.3
6	Southern latitudes, winter	6%	13	130	480	190	810	6.0	157	1025	81	−15	0.8
7	Central Siberia, summer	14%	14	100	430	190	730	4.5	147	1008	74	10	−0.4
8	Northeastern Siberia, summer	20%	13	70	360	160	600	4.0	127	1011	61	11	−0.6
9	Northeastern Siberia, winter	5%	27	110	190	100	430	3.2	148	1034	74	−31	0.8
10	Arctic, winter	7%	27	90	240	100	450	2.7	145	1016	81	−13	0.4

1 Number concentration in the diameter range 15–30 nm, in cm^{-3}
2 Number concentration in the diameter range 30–60 nm, in cm^{-3}
3 Number concentration in the diameter range 60–200 nm, in cm^{-3}
4 Number concentration in the diameter range 200–800 nm, in cm^{-3}
5 Particle mass concentration in $\mu g\,m^{-3}$ (assuming a density of $1.6\,g\,cm^{-3}$)
6 CO mixing ration in ppb
7 Season index, +1=mid-winter, −1=mid-summer.

ACPD
11, 1153–1188, 2011

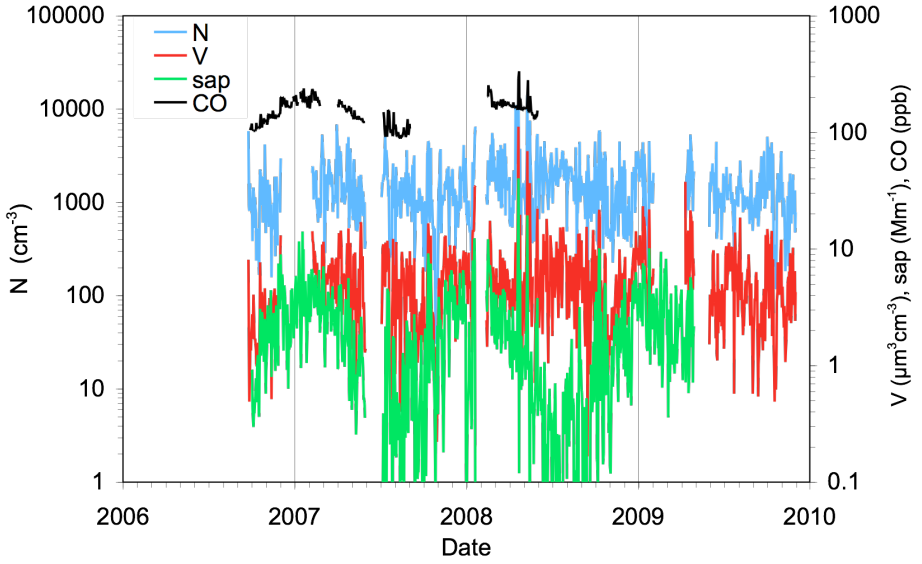

Fig. 1. Daily averages of total number (N, cm^{-3}), total volume (V, $\mu m^3\,cm^{-3}$), particulate absorption at 570 nm wavelength (σ_{ap}, $M\,m^{-1}$; average of 50 m and 300 m), and CO (CO, ppb) in 300 m at ZOTTO, Siberia.

ACPD
11, 1153–1188, 2011

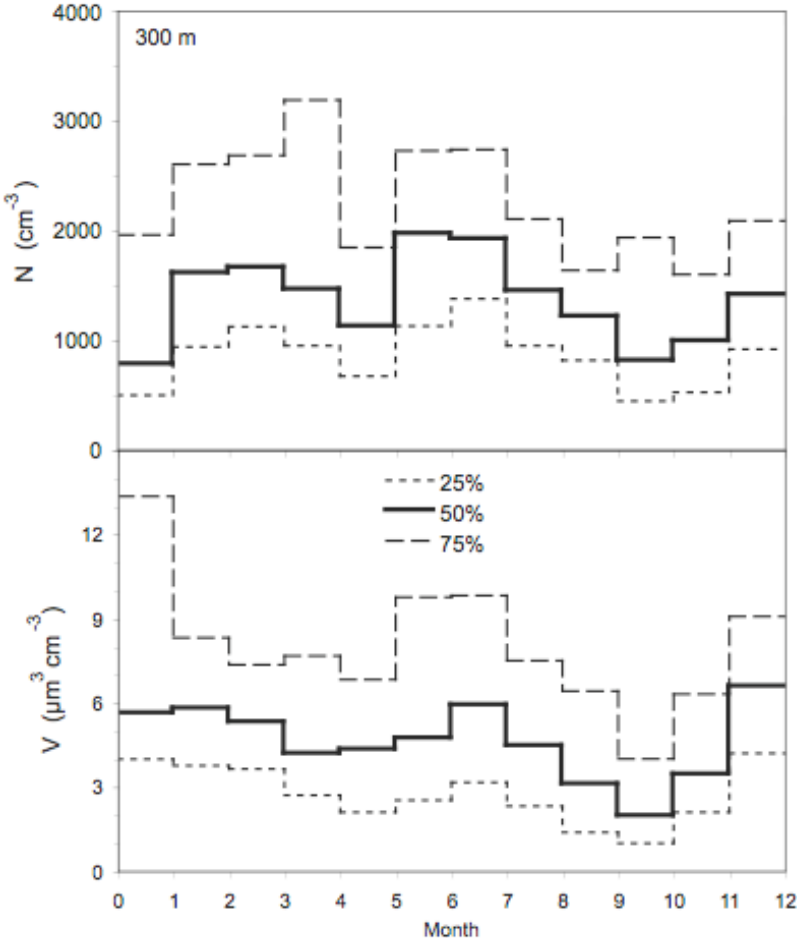

Fig. 2. Monthly percentiles of total number (N, cm^{-3}), and total volume (V, μm^3 cm^{-3}) in 300 m height at ZOTTO, Siberia taken over the time period September 2006 through January 2010.

ACPD
11, 1153–1188, 2011

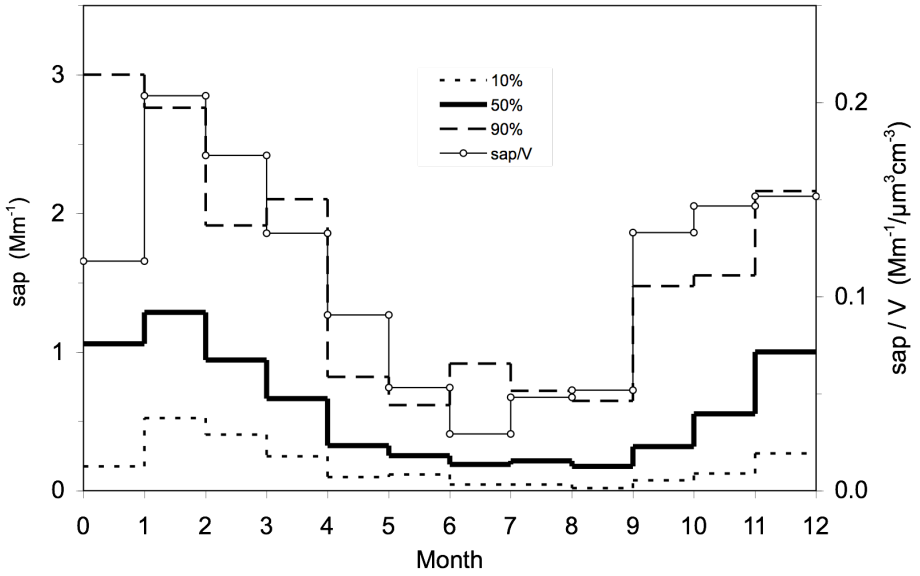

Fig. 3. Monthly percentiles 10%, 50%, and 90% of particulate absorption coefficients (σ_{ap} in $M\,m^{-1}$) at 570 nm wavelength in 300 m height at ZOTTO, Siberia taken over the time period September 2006 through April 2009; averages of 50 m and 300 m. The ratio of median σ_{ap} to median volume concentration is depicted as thin line with circles.

ACPD
11, 1153–1188, 2011

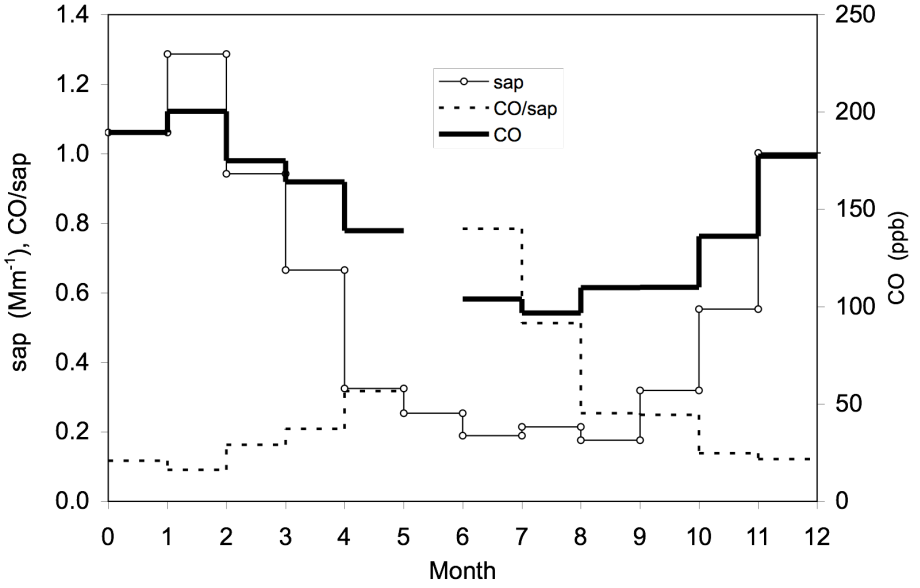

Fig. 4. Monthly medians of the particulate absorption coefficient at 570 nm (σ_{ap}, M m^{-1}), CO concentrations (ppb), and the ratio CO/σ_{ap} at ZOTTO; averages of 50 m and 300 m.

ACPD
11, 1153–1188, 2011

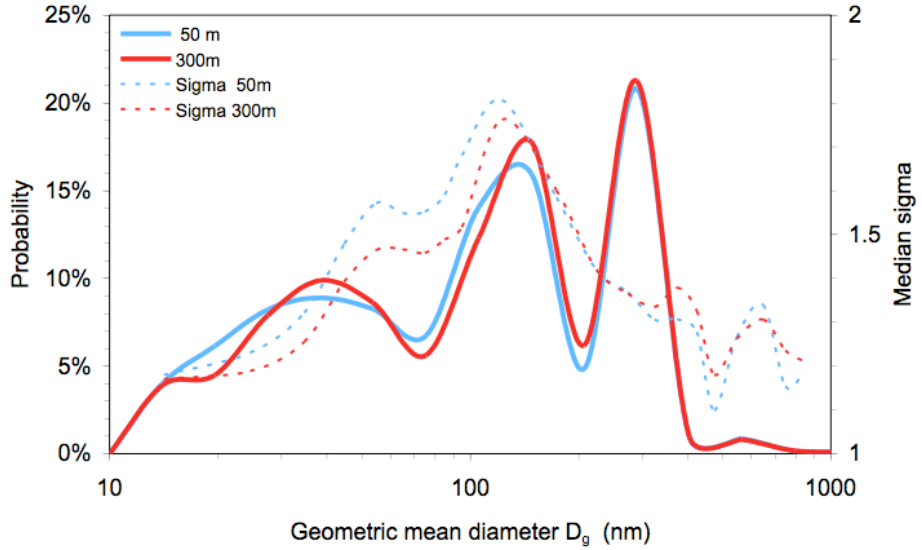

Fig. 5. Frequency distribution of modal diameters of 1-h-median number size distributions taken at 50 m and 300 m height at ZOTTO (full lines). The size distributions were fitted with a maximum of three lognormal modes in the range 10–1000 nm modal diameters. The dashed lines give median values of geometric standard deviations as a function of geometric mean diameter.

ACPD
11, 1153–1188, 2011

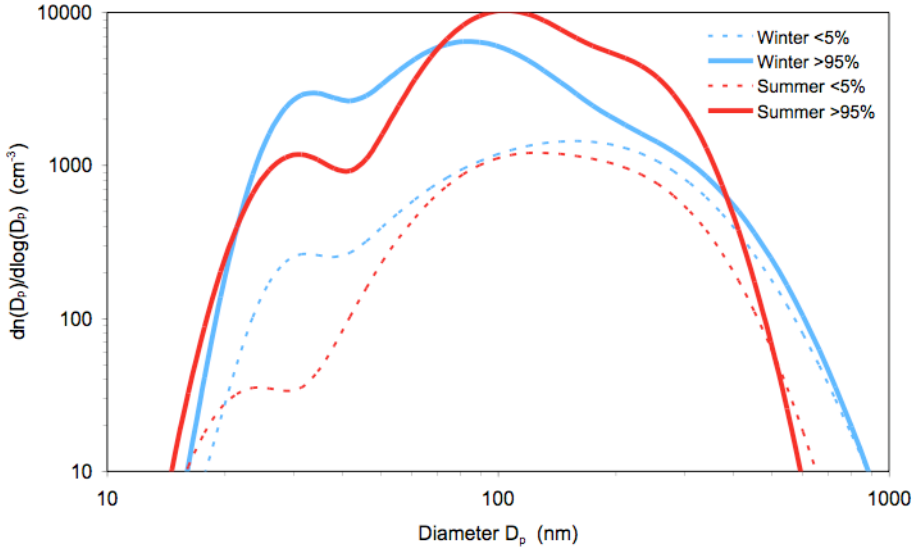

Fig. 6. Median number size distributions in air masses with the smallest (<5%, dashed) and highest (>95%, full lines) values of the total number concentration at ZOTTO in summer (May through August), and winter (November through February).

ACPD
11, 1153–1188, 2011

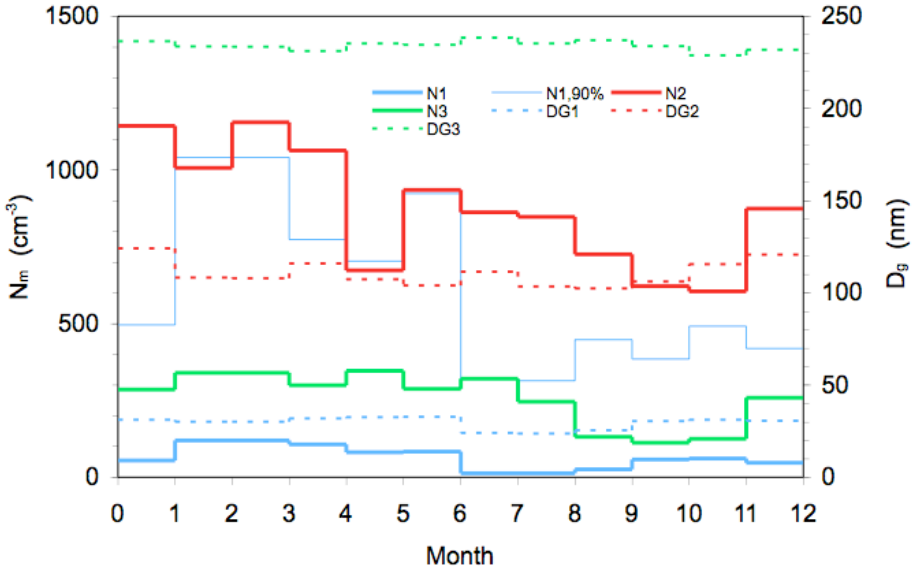

Fig. 7. Monthly medians of the total particle numbers N_m (N_1–N_3, cm^{-3}, full lines) and geometric mean diameters D_g (D_{g1}–D_{g3}, nm, dashed lines) of three lognormal distributions fitted to the particle number size distributions measured at ZOTTO. The 90% percentile of N_1 is drawn as thin full line.

ACPD
11, 1153–1188, 2011

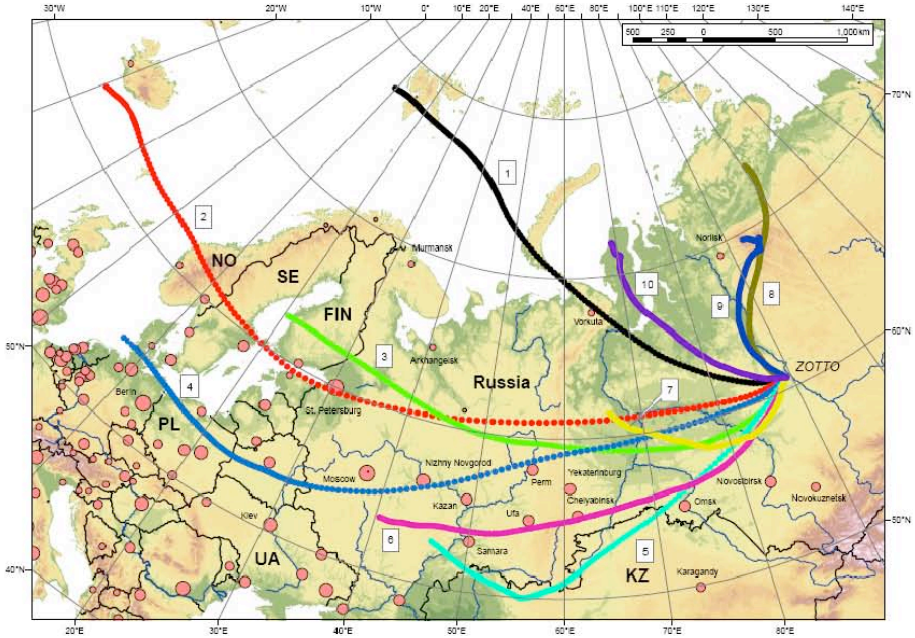

Fig. 8. Mean back trajectories arriving at ZOTTO as obtained from *k*-means cluster analysis. The travel time of all trajectories is 144 h. Circles indicate urban agglomerations with population in proportion to the diameter of the symbol.

ACPD
11, 1153–1188, 2011

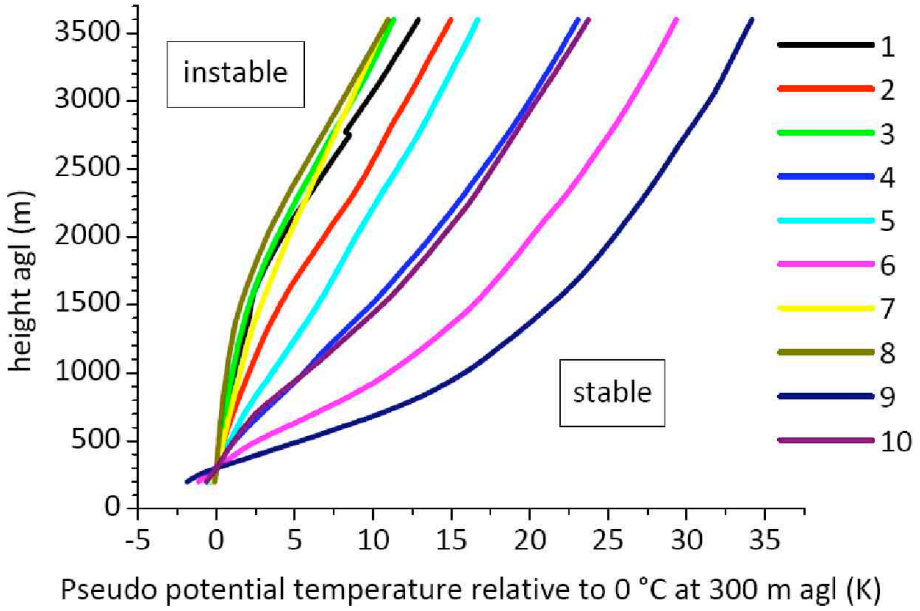

Fig. 9. Mean profiles of pseudo-potential temperature (θ_v) for the ten trajectory clusters as a function of height. The profiles were part of the clustered variables in the *k*-means cluster analysis, and originated from the 19:00 LT radio sounding at Bor. The profiles allow a clear distinction between more and less stable stratification.

ACPD
11, 1153–1188, 2011